

SWAMP: A Two-dimensional Hydrodynamic and Quality Modeling Platform for Shallow Waters

P. Covelli, S. Marsili-Libelli, G. Pacini
Department of Systems and Computers,
University of Florence,
Via S. Marta, 3-50139 Firenze, Italy

Received 30 May 2000; accepted 14 August 2001

Water quality two-dimensional models are often partitioned into separate modules with separate hydraulic and biological units. In most cases this approach results in poor flexibility whenever the biological dynamics has to be adapted to a specific situation. Conversely, an integrated approach is pursued in this article, producing a two-dimensional hydraulic-water quality model, named Shallow Water Analysis and Modeling Program (SWAMP) designed for shallow water bodies. The major objective of the work is to create a comprehensive two-dimensional water quality assessment tool, based on an open framework and combining easy programming of additional procedures with a user-friendly interface. The model is based on the numerical solution of the partial differential equations describing advection-diffusion and biological processes on a two-dimensional rectangular finite elements mesh. The hydraulics and advection-diffusion modules model were validated both with experimental tracer data collected at a constructed wetland site and a comparison with a commercial hydrodynamic software, showing good agreement in both cases. Moreover, the model was tested in critical conditions for mass conservation, such as time-varying wet boundary, showing a considerable numerical robustness. In the last part of the article water quality simulations are presented, though validation data are not yet available. Nevertheless, the observed model response demonstrates general consistency with expected results and the advantages of integrating the hydraulic and quality modules. The interactive graphical user interface (GUI) is also shown to represent a simple and effective connective tool to the integrated package. © 2002 Wiley Periodicals, Inc. *Numer Methods Partial Differential Eq* 18: 663–687, 2002; DOI 10.1002/num.10014

Keywords: water quality; shallow waters; finite differences; two-dimensional; hydrodynamics; advection-diffusion; tracer

1. INTRODUCTION

Shallow water bodies are becoming more and more important as environmentally sensitive areas, for their role in biodiversity conservation, eutrophication, and pollution prevention. Hence the need of sophisticated and yet simple to use modeling tools as decision support systems.

Correspondence to: S. Marsili-Libelli, Department of Systems and Computers, University of Florence, Via S. Marta, 3-50139 Firenze, Italy (e-mail: marsili@ingfi1.ing.unifi.it)

© 2002 Wiley Periodicals, Inc.

Two-dimensional water quality problems are usually approached in a separate way, with independent hydraulics and biological processes. A very accurate two-dimensional hydraulic model, designed for hydrodynamic problems, is often used to define the velocity field [1, 2]. Then an additional software, provided as an additional block to the hydraulic model or completely disjointed, is added to perform the water quality analysis. In most cases this approach results in poor flexibility whenever the biological dynamics has to be adapted to a specific situation. The primary aim of the article is to bring a contribution of convergence among tools from the traditional fields of environmental, hydraulic, and computer engineering to produce a self-contained water quality analysis package with enhanced interactive capabilities. Therefore the quality of the resulting product should be assessed not only in terms of computational performance, but also of interface efficiency and seamless integration among differing environments. It will be shown how this has been achieved through advancements in the implementation of hydrodynamics and biochemical kinetics modeling, and the design of a simple and efficient user interface. The model is based on the numerical solution of the partial differential equations describing advection-diffusion and biological processes on a two-dimensional rectangular finite elements mesh. The software, named Shallow Water Analysis and Modelling Program (SWAMP), includes pre- and postprocessing routines developed to facilitate morphological data input and to present the hydraulic and water quality simulation results as two- or three-dimensional plots. The most relevant modules implemented in the preprocessing package are the three-dimensional interpolation of the topographic points and an interactive numerical mesh generator. Through this module the user can visually appreciate the effects of discretization, balancing the spatial accuracy with the total number of grid elements, with obvious implications on memory requirements and computational complexity. Both the advection-diffusion and quality models were developed in MatLab 5.3, using its Graphic User Interface, whereas C++ subroutines for the main solution algorithm were compiled and linked as MEX-files. This implementation enhances the computational performance of the model, reducing the run time by two orders of magnitude compared to plain MatLab implementation, remaining at the same time absolutely transparent to the user.

II. MODEL STRUCTURE

In addition to the user interface, SWAMP consists of three parts, representing the free surface two-dimensional flow movement, the advective-diffusion, and the pollutant transformation processes. They are now briefly reviewed.

A. Hydrodynamics

The hydrodynamic behavior may be described by the well-known Shallow Water St. Venant complete equations (SWE). In a nonconservative setting the flux equations may be expressed as

$$\frac{\partial h}{\partial t} + \frac{\partial M_x}{\partial x} + \frac{\partial M_y}{\partial y} = 0 \quad (2.1)$$

$$\frac{\partial M_x}{\partial t} + \frac{\partial(u_x M_x)}{\partial x} + \frac{\partial(u_y M_x)}{\partial y} + gh \frac{\partial H}{\partial x} + \frac{1}{\rho} \tau_x + ha_{w,x} = 0 \quad (2.2)$$

$$\frac{\partial M_y}{\partial t} + \frac{\partial(u_x M_y)}{\partial x} + \frac{\partial(u_y M_y)}{\partial y} + gh \frac{\partial H}{\partial y} + \frac{1}{\rho} \tau_y + ha_{w,y} = 0 \quad (2.3)$$

where h is the flow depth; g is the gravity acceleration; H is the total surface elevation above a reference height; ρ is the water density; M_x, M_y are the flows in the x and y directions, respectively; u_x, u_y are the flow velocities in the x and y directions; $a_{w,x}, a_{w,y}$ are the wind-induced accelerations in the x and y directions. The bed shear stress components in the x and y directions may be expressed through the Manning equation as

$$\tau_x = \frac{\rho g n^2 u_x \sqrt{u_x^2 + u_y^2}}{h^{1/3}} \tag{2.4}$$

$$\tau_y = \frac{\rho g n^2 u_y \sqrt{u_x^2 + u_y^2}}{h^{1/3}} \tag{2.5}$$

where n is the Manning roughness coefficient. The wind-induced acceleration terms are expressed as

$$a_{w,x} = \frac{C_d \rho_a}{h \rho} w^2 \cos(\alpha) \tag{2.6}$$

$$a_{w,y} = \frac{C_d \rho_a}{h \rho} w^2 \sin(\alpha), \tag{2.7}$$

where C_d is a dimensionless drag coefficient, ρ_a is the air density; w is the wind speed; α is the angle between the x axis and wind direction expressed in decimal degrees. From Eqs. (2.6)–(2.7) it can be seen that the wind action has been modeled simply as an additional energy contribution transferred to the water motion, neglecting the possibility of wind-induced surface waves, which are likely to occur only for wind velocity in excess of 15 m/s [3]. Based on the assumption of uniform velocity distributions u_x and u_y along the water column, the average wind effect along the vertical axis has been assessed, concluding that the wind drift underestimation is compensated by overestimation of induced bottom velocities.

B. Pollutant Dynamics

The pollutant dynamics are expressed by the mass balance for a stationary control volume through which the fluid flows as a result of advection, diffusion, and chemical transformations. The complete pollutant dynamics can thus be written in two dimensions as

$$\frac{\partial C}{\partial t} = -u_x \frac{\partial C}{\partial x} - u_y \frac{\partial C}{\partial y} + D_x \frac{\partial^2 C}{\partial x^2} + D_y \frac{\partial^2 C}{\partial y^2} - f(C) + C_i(x, y, t) \tag{2.8}$$

where C is the pollutant concentration (mg/l); u_x, u_y are the advection velocities in the x and y directions respectively, D_x, D_y are the diffusion coefficients; $f(C)$ is the generic kinetic term, which will be specified for each water quality component, and $C_i(x, y, t)$ is the exogenous loading rate for each pollutant.

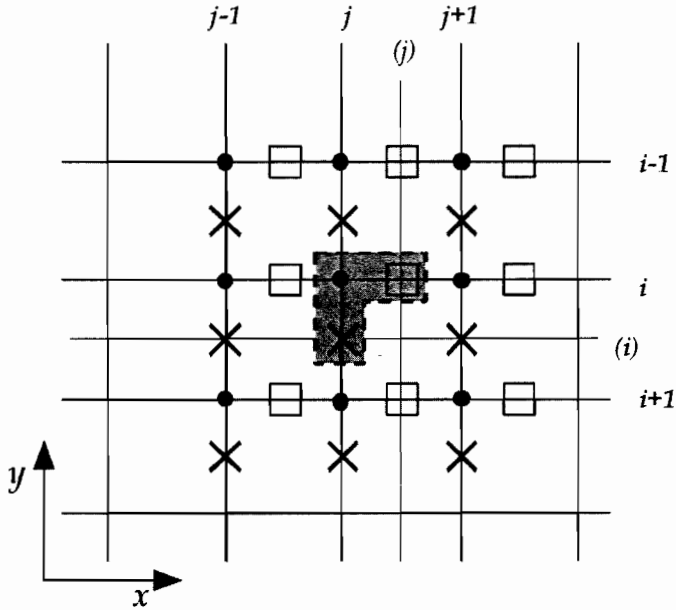


FIG. 1. C-shaped solution region for the SWE Eqs. (2.1)–(2.3) in a shallow field. □, M_x grid points for space differences; ×, M_y grid points for space differences; ●, h grid points for time differences.

III. NUMERICAL METHODS

Numerical computations for the hydraulic flow uses the C-shaped explicit centered scheme. The horizontal two-dimensional advective-diffusion equation solution algorithm is derived from on the Mac Cormack predictor-corrector scheme [4].

A. Numerical Scheme for Two-dimensional Surface Flow

An explicit centered finite difference scheme has been used to solve the full St. Venant equations in the form of Eqs. (2.1)–(2.3). This method is based on that originally proposed by Iwasa and Inoue [5] and has been adapted for modeling hydraulic flow in shallow water bodies. This scheme operates on a C-shaped region using a centered-time/centered-space strategy as shown in Fig. 1.

Estimates of the three hydrodynamic variables proceeds as follows: if the spatial node numbers i and j refer to h -grid points, then the flows M_x and M_y having the same index at the distance $\Delta x/2$ and $\Delta y/2$, respectively, from the h -grid point, are as shown in Fig. 1. The shaded line contains the grid points with node numbers i and j . From a numerical point of view, Eqs. (2.2)–(2.3) are used to obtain the unknown values of $M_x^{t+\Delta t}$ and $M_y^{t+\Delta t}$ with M_x^t , M_y^t , and h^t specified as initial conditions or computed over all nodes of the domain at the previous time step. The computed values $M_x^{t+\Delta t}$ and $M_y^{t+\Delta t}$ are replaced in Eq. (2.1) to yield $h^{t+\Delta t}$. The discrete-form of the continuity equation is the following:

$$\frac{h^{t+\Delta t}(i,j) - h^t(i,j)}{\Delta t} + \frac{M_x^{t+\Delta t}(i,j) - M_x^{t+\Delta t}(i,j-1)}{\Delta x} + \frac{M_y^{t+\Delta t}(i,j) - M_y^{t+\Delta t}(i-1,j)}{\Delta y} = 0, \quad (3.1)$$

where i and j are the spatial node numbers in the y and x directions, respectively; t is the time step index, and Δx , Δy the grid size. The discrete-time form of the various terms in the motion equations in the x and y directions are

$$\frac{\partial M_x}{\partial t} = \frac{M_x^{t+\Delta t}(i,j) - M_x^t(i,j)}{\Delta t} \tag{3.2}$$

$$\frac{\partial(u_x M_x)}{\partial x} = \frac{1}{\Delta x} \frac{1}{h'(i,j+1)} \left(\frac{M_x^t(i,j) - M_x^t(i,j+1)}{2} \right)^2 - \frac{1}{\Delta x} \frac{1}{h'(i,j)} \left(\frac{M_x^t(i,j) + M_x^t(i,j-1)}{2} \right)^2 \tag{3.3}$$

$$\begin{aligned} \frac{\partial(u_y M_x)}{\partial y} = & \frac{1}{\Delta y} \frac{(M_x^t(i,j) + M_x^t(i+1,j))(M_y^t(i,j) + M_y^t(i,j+1))}{h'(i,j) + h'(i,j+1) + h'(i+1,j+1) + h'(i+1,j)} \\ & - \frac{1}{\Delta y} \frac{(M_x^t(i,j) + M_x^t(i-1,j))(M_y^t(i-1,j) + M_y^t(i-1,j+1))}{h'(i,j) + h'(i,j+1) + h'(i-1,j+1) + h'(i-1,j)} \end{aligned} \tag{3.4}$$

$$gh \frac{\partial H}{\partial x} = g \left(\frac{h'(i,j) + h'(i,j+1)}{2} \right) \left(\frac{H^t(i,j+1) - H^t(i,j)}{\Delta x} \right) \tag{3.5}$$

$$\frac{1}{\rho} \tau_x = \frac{gn^2(i,j) \left(\frac{M_x^{t+\Delta t}(i,j) + M_x^t(i,j)}{h'(i,j) + h'(i,j+1)} \right) \sqrt{(u_x^t(i,j))^2 + u_y^t(i,j)^2}}{h'(i,j) + h'(i,j+1)^{1/3}} \tag{3.6}$$

$$\frac{\partial M_y}{\partial t} = \frac{M_y^{t+\Delta t}(i,j) - M_y^t(i,j)}{\Delta t} \tag{3.7}$$

$$\frac{\partial(u_x M_y)}{\partial x} = \frac{1}{\Delta y} \frac{1}{h'(i+1,j)} \left(\frac{M_y^t(i,j) - M_y^t(i+1,j)}{2} \right)^2 - \frac{1}{\Delta y} \frac{1}{h'(i,j)} \left(\frac{M_y^t(i,j) + M_y^t(i-1,j)}{2} \right)^2 \tag{3.8}$$

$$\begin{aligned} \frac{\partial(u_x M_y)}{\partial y} = & \frac{1}{\Delta y} \frac{(M_y^t(i,j) + M_y^t(i,j+1))(M_x^t(i+1,j) + M_x^t(i,j+1))}{h'(i,j) + h'(i,j+1) + h'(i+1,j+1) + h'(i+1,j)} \\ & - \frac{1}{\Delta y} \frac{(M_y^t(i,j) + M_y^t(i,j-1))(M_x^t(i,j-1) + M_x^t(i+1,j-1))}{h'(i,j) + h'(i+1,j) + h'(i+1,j-1) + h'(i,j-1)} \end{aligned} \tag{3.9}$$

$$gh \frac{\partial H}{\partial y} = g \left(\frac{h'(i,j) + h'(i+1,j)}{2} \right) \left(\frac{H^t(i+1,j) - H^t(i,j)}{\Delta y} \right) \tag{3.10}$$

$$\frac{1}{\rho} \tau_y = \frac{gn^2(i,j) \left(\frac{M_y^{t+\Delta t}(i,j) + M_y^t(i,j)}{h'(i,j) + h'(i+1,j)} \right) \sqrt{(u_x^t(i,j))^2 + u_y^t(i,j)^2}}{h'(i,j) + h'(i+1,j)^{1/3}} \tag{3.11}$$

For centered differences in the space and time domains, the stability criterion of Courant-Friedrichs and Lewy is imposed:

$$\Delta t < \frac{\min\{\Delta x, \Delta y\}}{\sqrt{2gh}} \tag{3.12}$$

B. MacCormack Method

The Mac Cormack scheme has been used to solve the advective-diffusion equation. This numerical resolution method is widely used for solving advection-diffusion problems because of its ease of programming and good numerical efficiency when compared to other second-order schemes [3, 6]. The representation of the two-dimensional pollutant transport equation using conservative two-step predictor-corrector second-order scheme is

Predictor(Forward-difference)

$$S_1 = \frac{-u'_x(i,j+1)C(i,j+1) - u'_x(i,j)C(i,j)}{\Delta x} + \frac{-u'_y(i+1,j)C(i+1,j) - u'_y(i,j)C(i,j)}{\Delta y} + D_x \frac{C(i,j+1) - 2C(i,j) + C(i,j-1)}{\Delta x^2} + D_y \frac{C(i+1,j) - 2C(i,j) + C(i-1,j)}{\Delta y^2} \tag{3.13}$$

$$\tilde{C}^{t+\Delta t}(i,j) = C^t(i,j) + S_1 \Delta t \tag{3.14}$$

Corrector(Backward-difference)

$$S_2 = \frac{-u'_x(i,j)\tilde{C}^{t+\Delta t}(i,j) - u'_x(i,j-1)\tilde{C}^{t+\Delta t}(i,j-1)}{\Delta x} + \frac{-u'_y(i,j)\tilde{C}^{t+\Delta t}(i,j) - u'_y(i-1,j)\tilde{C}^{t+\Delta t}(i-1,j)}{\Delta y} + D_x \frac{\tilde{C}^{t+\Delta t}(i,j+1) - 2\tilde{C}^{t+\Delta t}(i,j) + \tilde{C}^{t+\Delta t}(i,j-1)}{\Delta x^2} + D_y \frac{\tilde{C}^{t+\Delta t}(i+1,j) - 2\tilde{C}^{t+\Delta t}(i,j) + \tilde{C}^{t+\Delta t}(i-1,j)}{\Delta y^2} \tag{3.15}$$

$$C^{t+\Delta t}(i,j) = C^t(i,j) + \frac{S_1 + S_2}{2} \Delta t \tag{3.16}$$

This solution results in a highly accurate numerical scheme, particularly if the diffusion mechanisms prevail over advection, as is often the case with shallow waters.

IV. BOUNDARY CONDITION

A. Dry-wetting Problem

Shallow water bodies, such as wetland, lagoons, or unstratified lakes are usually associated with relatively mild bottom slopes. For this reason, very small variations of the water depth can

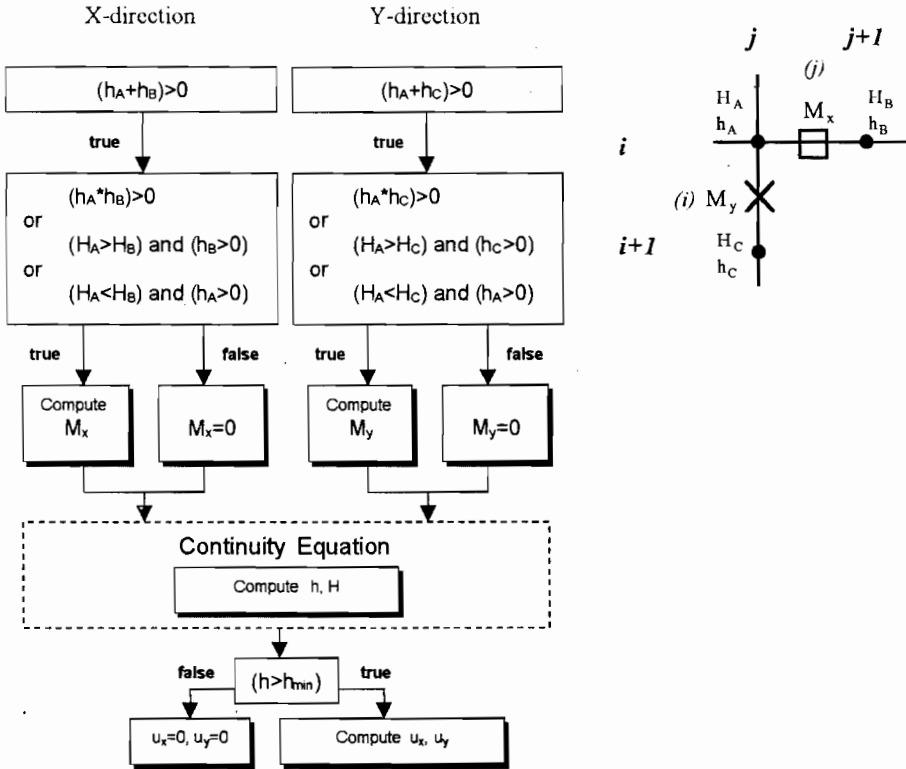


FIG. 2. Logical algorithm for the "dry-wet" problem.

significantly change the wetted area. To model this, a dynamic subgroup of domain cells are considered, which may change their water depth from zero to a finite value over one time step. This is the usually referred to as the "dry-wetting problem." The introduction of a variable domain is translated into code using logical controllers on water depth, not only looking at dry-wet cells, but also considering the state of the adjacent elements. This problem considerably increases the overall complexity of the algorithm. Furthermore, when a dry-wet cells switches from dry to wet condition, it is included in the set for which the velocity field is computed. To prevent numerical instability, the velocity components at each node are computed only if the water depth is deeper than a threshold value, generally assumed to be in the 5- to 50-mm range.

Figure 2 shows the logical organization of the algorithm in selecting the wet boundary grid nodes in which the velocity should be computed. This scheme yields the increase of water depth at each time step using the continuity equation whenever possible, until the minimum water depth value (h_{min}) is reached so that the velocity components can be calculated. Even if these logical controls bring a slight increase in computational time, they are instrumental in modeling the dynamics of changing volumes in shallow water areas.

B. Boundary Condition for the Hydraulic Equations

Boundary conditions for unsteady hydraulic models are generally difficult to define because natural systems such as estuaries or lagoons usually do not have a constant morphological boundary. This problem is very common in coastal hydrodynamic models, in which the

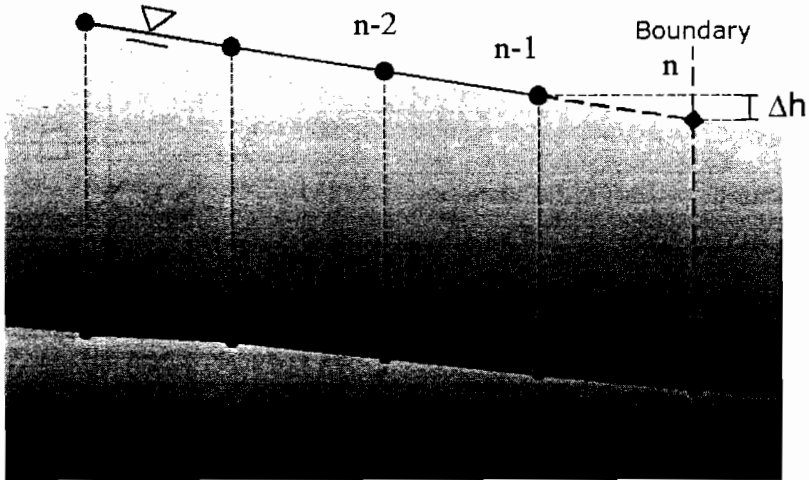


FIG. 3. Boundary hydraulic condition.

numerical boundaries, being far from the coast, are defined in terms of momentum. Using a rectangular mesh, the four sides of the domain are assumed to be open boundaries, regardless of the actual location of the outlet. These four interfaces of the numerical grid are treated separately from the main algorithm. This allows easy handling and editing of the rules that approximate velocities and water elevations along the domain border. Free surface water elevation, the velocity normal to the boundary or a rating curve are possible choices for different applications. This flexibility is very useful in applying the model to real-world situations because the equation that best represents the actual boundary conditions can be directly implemented on a case-by-case basis. A simple open boundary condition that allows model operation with minimum input data is implemented by default in the code and consists of an extrapolation of the free water surface. As shown in Fig. 3, the local slope of the free surface is first evaluated at the $(n - 1)$ point and then extrapolated to the boundary point (n) . If the bottom slope does not change sharply near the boundary, this approach is similar to assuming uniform velocity. Several numerical simulations have shown that this simple boundary condition yields good agreement with the results obtained with more accurate representations whenever the bottom morphology does not change sharply in the neighborhood of the domain border.

C. Boundary Conditions for Advection-Diffusion Equation

Boundary conditions for the advection-diffusion equation are quite simple to define because they can be expressed in terms of forward or backward differences, instead of centered differences as with the internal points. Because the Mac Cormack method was used to solve the advection-diffusion equation, a half-time step value was introduced to compute the concentration in the boundary points, as already explained in Section B.

V. HYDRODYNAMIC MODEL VALIDATION

In order to assess the consistency of the hydrodynamic computational scheme, tracer data were used from an experimental basin, which will become a constructed wetland, located on the left

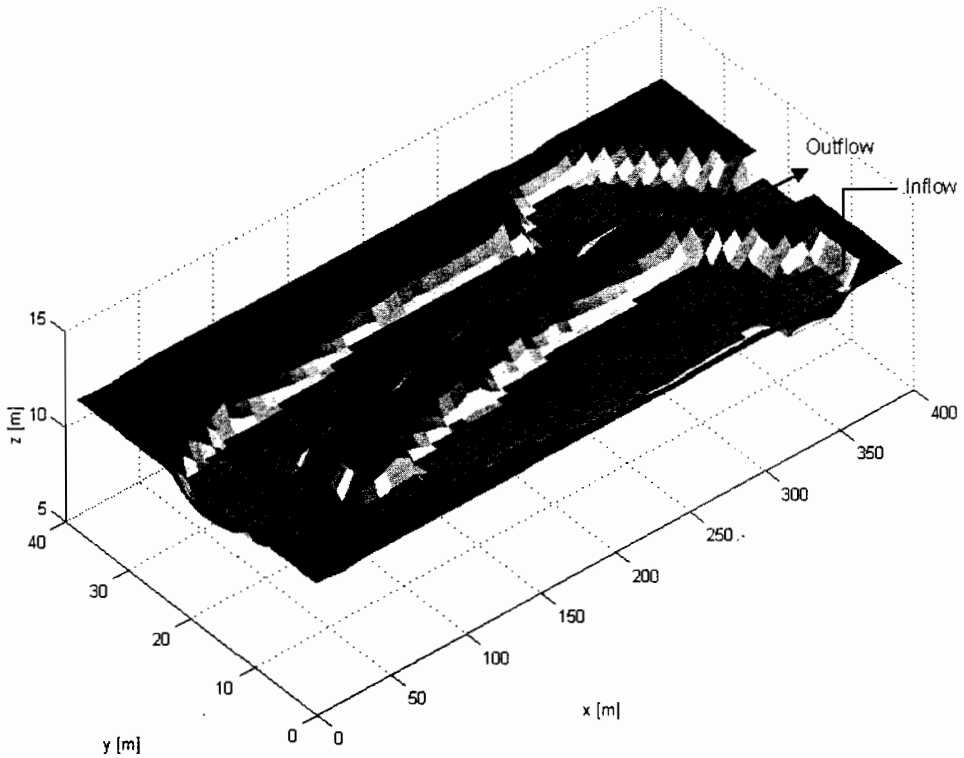


FIG. 4. Finite difference model representation of the constructed wetland used for the tracer experiments.

embankment of the Po River near Rovigo, Italy. This U-shaped shallow area is approximately 800 m in length and 30 m across. The flow and the water depth are controlled by a system of pumps and weirs. Even if this artificial basin is far from being the proper application for a shallow water model, given its shape, the fact that the hydrodynamic processes can be completely controlled is very useful for the validation procedure. The experimental conditions for the tracer experiments were an input flow of 80 l/s and a maximum depth of 1.30 m, with an average water depth of 0.8 m. A digital elevation model of the terrain was generated by the preprocessing routine, to be described in Section VIII, using a three-dimensional interpolation over 2,000 topographic points. Figure 4 shows the finite element model representation of the site using a rectangular 2×8 m mesh.

The validation of the model and related numerical methods was performed in two steps. First a tracer experiment was used to check the ability of the model to reproduce diffusive behavior of the shallow water basin. Then the same system was modeled with MIKE21 (a widespread two-dimensional hydraulic modeling package developed by DHI Software, Denmark), and the two simulations were compared. Like SWAMP, MIKE21 solves the two-dimensional SWE on a rectangular grid, but the momentum conservation equations include the eddy viscosity contribution. The numerical solution is obtained through an implicit ADI finite difference scheme of second-order accuracy. A simulation was performed with a constant input flow rate until, after 2 days, a steady state was reached. Because the velocity field was not experimentally recorded, the model hydrodynamic assessment was performed using a tracer experiment described in next section.

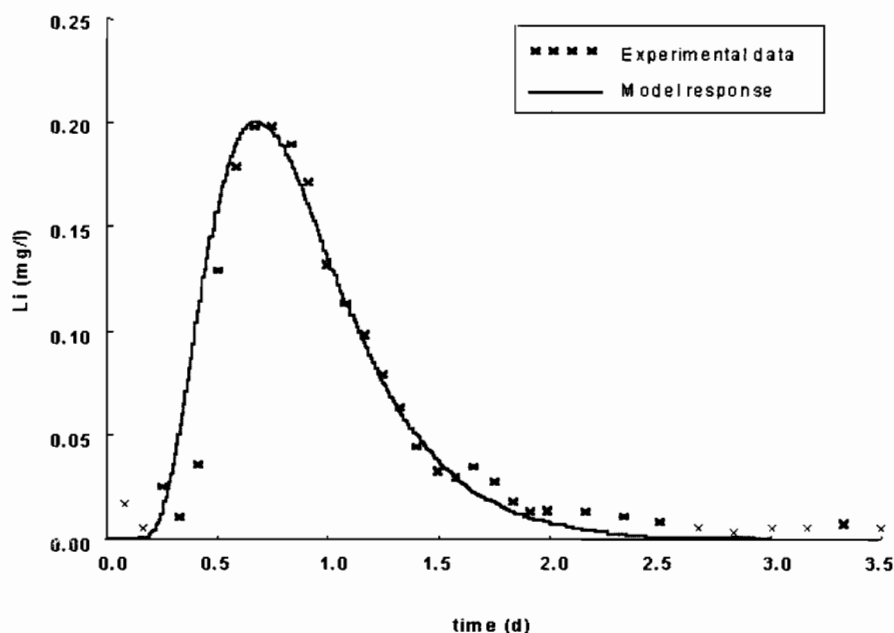


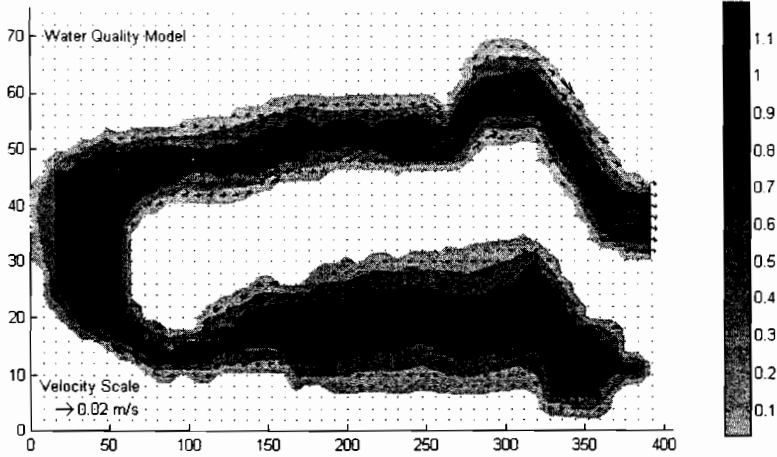
FIG. 5. Lithium spill trace experiment for the calibration of the diffusion coefficient in the *Po* wetland: comparison between model response and experimental data with the calibrated value $D = 0.4532 \text{ m}^2 \text{ s}^{-1}$.

A. Experimental Tracer Calibration

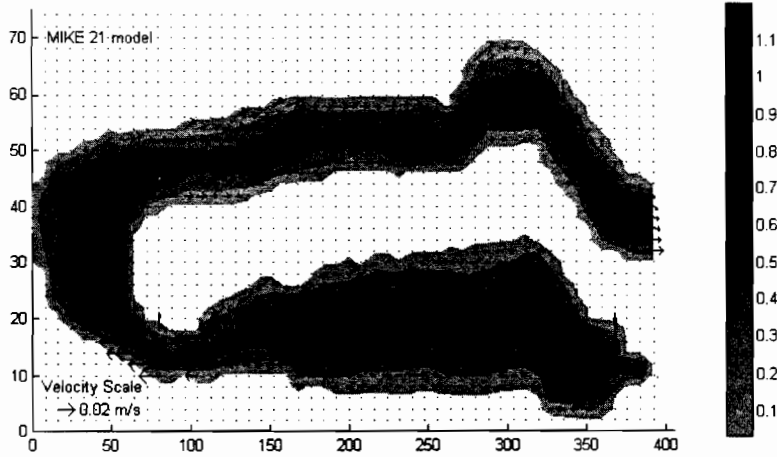
A spill tracer experiment is a widely used technique for testing the advection-diffusion characteristics of a hydrodynamic model. Lithium tracer was used as a spill injection in the inflow of the constructed wetland, and the output concentration was recorded. The same experiment was then simulated using the hydrodynamic module and adjusting the dispersion-diffusion coefficient D , assumed the same in the x and y direction, in order to minimize the squared sum of difference between the experimental data and the model response. This was performed through a numerical search described elsewhere [7] and an optimal value of $D = 0.4532 \text{ m}^2/\text{s}$ was obtained. This value falls within the preferred range indicated in the literature for similar water bodies [8, 9]. The agreement between experimental tracer data and calibrated model is shown in Fig. 5. A global lithium mass balance was also performed as a check. The injected mass was 1305 g, and the total mass recorded at the outlet, after the 3-day experiment, summed up to 1230 g. The missing fraction, though negligible, could be justified with a limited uptake by the submerged macrophytes for which lithium plays a role similar to potassium.

B. Comparison with MIKE21 Simulation

In order to evaluate its performance, the model was compared with a well-established two-dimensional hydrodynamic model, MIKE21. Figure 6 compares the velocity fields and bathymetries from the present model to that obtained with MIKE21. For the latter simulation, an eddy viscosity value of 0.20 was used. The velocity fields given by the two models are in good agreement, especially considering the strong sensitivity of MIKE21 to eddy viscosity, which may produce some inaccuracies for the predicted velocity, both in magnitude and direction, for



a)



b)

FIG. 6. Comparison between the flow velocity fields obtained from the proposed water quality model and MIKE21 model.

very shallow conditions. The average velocities lie in the range of 0.004 to 0.008 m/s, so the low advective condition may amplify inaccuracies in the numerical resolution scheme of both models. However, this seems to be better handled by the proposed model, which is conceived for shallow waters with very low flows. Further, it can be noticed in Figure 6(b) that for MIKE21 the water velocity distribution produced by MIKE21 does not follow the expected parabolic profile along a cross section, and in some cases it is not tangent to the dry boundary. These shortcomings do not appear in the proposed model simulation [Fig. 6(a)].

As a consequence of the low water velocities, the effect of diffusion is comparable with the advective process. After 3 days it can be assumed that the lithium spill is completely washed out from the wetland so that it is possible to evaluate the mass conservation during the simulation.

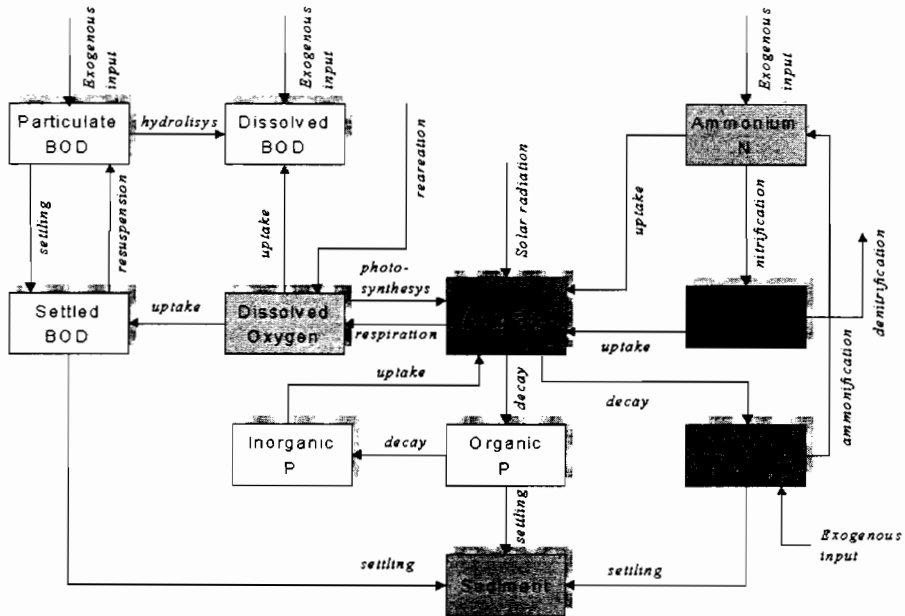


FIG. 7. Structure of the water quality model.

VI. WATER QUALITY MODELING

A. Pollutant Dynamics

The pollutant dynamics of Eq. (3.1) is now considered again to specify the chemical kinetic term $f(C)$. A large number of interactions between molecules and living organisms contribute to the dynamics of water quality [9–13] and only the most important of them are considered in this model, which has a structure similar to QUAL2 [14]. Because the research is aimed at modeling shallow water bodies, rather than fast-flowing rivers or stratified lakes, the main characteristics of these systems are an aerobic environment with low advection velocities in the two horizontal directions. As a consequence, high oxygen consumption, long retention times, possible eutrophication, and a high settling rate have been considered. Therefore, the processes included in the model are the transformation of carbonaceous compounds, expressed as BOD, the inclusion of nitrogen and phosphorous as the main nutrients, both in inorganic and organic form, algae in the water column, and decomposition at the bottom. The structure of the water quality model is shown in Fig. 7, where each transformation process (uptake, decay, settling, etc.) is indicated

$$\frac{\partial C}{\partial t} = -u_x \frac{\partial C}{\partial x} - u_y \frac{\partial C}{\partial y} + D_x \frac{\partial^2 C}{\partial x^2} + D_y \frac{\partial^2 C}{\partial y^2} - f(C) + C_i(x,y,t). \quad (6.1)$$

The main kinetics included in the model are now summarized.

B. BOD Kinetics

The removal processes of organic carbon both in the water column (dissolved fraction) and in the bottom (settled fraction) are well understood [9, 12, 14] and may be represented by the three forms of BOD: dissolved (BOD_d), directly available for the biodegradation, particulate BOD

(BOD_{pw}), which may be dissolved through hydrolysis, and settled BOD (BOD_{ps}), which may be either resuspended or biodegraded by bottom decomposers. The pertinent kinetic equations can be written as follows:

$$\frac{dBOD_d}{dt} = -K_b BOD_d + K_{hydr} BOD_{pw} \quad (6.2)$$

$$\frac{dBOD_{pw}}{dt} = -\frac{v_{sed}}{h} BOD_{pw} + \frac{v_{ris}}{h} BOD_{ps} - K_{hydr} BOD_{pw} \quad (6.3)$$

$$\frac{dBOD_{ps}}{dt} = \frac{v_{sed}}{h} BOD_{pw} - \frac{v_{ris}}{h} BOD_{ps} - K_{degsed} BOD_{ps}, \quad (6.4)$$

with

$$K_b(T) = K_b(20^\circ\text{C})\theta_b^{T-20} \quad (6.5)$$

$$K_b(20^\circ\text{C}) = 0.3 \left(\frac{h}{2.4} \right)^{-0.434} (\text{g}^{-1}) \quad \text{if } 0 < h < 2.4(\text{m})$$

$$K_b(20^\circ\text{C}) = 0.3(\text{g}^{-1}) \quad \text{if } h > 2.4(\text{m}), \quad (6.6)$$

where K_b is the reaction rate; K_{hydr} is the hydrolysis rate; K_{degsed} is the sediment degradation rate, v_{sed} is the settling velocity, and v_{ris} is the resuspension velocity. The relationship between the latter and the shear velocity was modeled by the sigmoid function of Eq. (6.7) with an upper bound depending on the dimensions and nature of the sediments. It is observed in practice that shear velocities in the order of 10 to 20 mm/s are enough to cause resuspension of the bottom sediments:

$$v_{ris} = v_{rismax} \frac{u^3}{u^3 + u_{crit}^3}. \quad (6.7)$$

C. DO Kinetic

The dissolved oxygen balance has two supply terms: the natural reaeration through the free surface, depending on the oxygen deficit ($DO_{sat} - DO$), and the oxygen production by algae through net photosynthesis ($P_{phyt} - R_{phyt}$). On the uptake side three consumption terms are considered: the oxygen demand for dissolved BOD degradation, which is the counterpart of the decay term in Eq. (6.2); the oxygen required for nitrification, which depends linearly on the available nitrate-N through the rate constant K_{nit} ; combined with an oxygen saturation term with half-constant K_o . The last term, representing oxidation of the bottom sediment is introduced as an unstructured rate term R_{sed} .

$$\frac{dDO}{dt} = K_{rear}(DO_{sat} - DO) + (P_{phyt} - R_{phyt})X_f - K_b BOD_d - 4.57K_{nit} \frac{DO}{DO + K_o} N_1 - R_{sed} \quad (6.8)$$

The DO_{sat} is the saturation oxygen concentration, depending primarily on the water temperature T [12]:

$$DO_{sat} = 14.652 - 0.41022T + 0.007991T^2 - 0.000077774T^3 \tag{6.9}$$

whereas the reaeration rate K_{rear} is a function of depth and stream velocity [12].

D. Nutrient/Plants Kinetics

Assuming that nitrogen and phosphorus are the only limiting factors, in addition to light, the relationship between algae biomass and nutrients, as shown in Fig. 7, can be written as

OrganicNitrogen

$$\frac{dN_o}{dt} = a_{na}K_dX_f - K_{min}N_o - K_{sed}N_o \tag{6.10}$$

AmmoniumNitrogen

$$\frac{dN_{amm}}{dt} = K_{min}N_o - \delta R_{phyt}X_f a_{na} - K_{nitr} \frac{DO}{DO + K_o} N_{amm} \tag{6.11}$$

NitrateNitrogen

$$\frac{dN_{nitr}}{dt} = K_{nitr} \frac{DO}{DO + K_o} N_{amm} - (1 - \delta)R_{phyt}X_f a_{na} - K_{dn} \frac{K_{NO3}}{K_{NO3} + DO} N_{nitr} \tag{6.12}$$

OrganicPhosphorus

$$\frac{dP_o}{dt} = a_{pa}K_dX_f - K_{min}P_o - K_{sed}P_o \tag{6.13}$$

InorganicPhosphorus

$$\frac{dP_i}{dt} = K_{min}P_o - a_{pa}K_gR_{cphyt}X_f \tag{6.14}$$

Algae

$$\frac{dX_f}{dt} = K_gR_{phyt}X_f - K_dX_f - K_{sedphyt}X_f \tag{6.15}$$

In Eq. (6.15) the first term represents the gross algae growth rate. This is expressed as the product of two separate rates, one depending on nutrients:

$$R_{phyt} = \frac{\delta N_{amm} + (1 - \delta)N_{nitr} P_i}{K_N + \delta N_{amm} + (1 - \delta)N_{nitr} P_i + K_P}, \quad (6.16)$$

and the other on temperature and light:

$$K_g = K_{g,20} 1.066^{T-20} \phi_l, \quad (6.17)$$

where the term

$$\phi_l = \frac{2.718f}{K_e h} (e^{-\alpha_1} - e^{-\alpha_0}) \quad \text{with } \alpha_1 = \frac{I_a}{I_s} e^{-K_e h}, \alpha_0 = \frac{I_a}{I_s} \quad (6.18)$$

is related to the photosynthetic oxygen producing term appearing in the dissolved oxygen balance Eq. (6.8) [9, 14]:

$$P_{phyt} = r_{oa} K_g, \quad (6.19)$$

where r_{oa} is the oxygen generated per unit mass of plant biomass produced and the algae respiration rate R_{phyt} is represented by

$$R_{phyt} = r_{oa} K_{ra} 1.08^{T-20}, \quad (6.20)$$

with K_{ra} being the algae respiration rate.

E. A Water Quality Simulation

The SWAMP water quality module is now demonstrated with a simple simulation of a two-dimensional eutrophication problems in which both nutrients and light play a significant role. Figure 8 shows a small shallow lake with two different water depth zones, with one monitoring point placed in the deep zone (MP1) and another in the shallow area (MP2). The aim of the simulation is to investigate the influence of water depth on algae dynamics and related nutrients uptake. Solar radiation cycle and water temperature are typical values for a June sunny day, at 44° northern hemisphere latitude. Literature values for the water quality parameters are used [9, 14]. A 10-day simulation was performed with no hydraulics or nutrient exogenous inputs. As expected, the algae growth rate is higher in the shallow area where radiation affects the whole water column, enhancing photosynthesis and nutrients removal. Here the maximum algae concentration is reached sooner than in the deep area, as shown in Fig. 9(a). On the seventh day decay begins to prevail over growth in the shallow area because nutrients have been depleted (phosphorus is the first limiting factor), whereas in the middle of the lake the growth is still predominant over decay until day 8. After 10 days the deep zone shows a higher concentration of chlorophyll-*a* due to the longer growth period [Fig. 9(b)]. Figure 10 shows the algae-nutrients time concentrations at the two monitoring points. As is often observed in practice, the growth rate slowdown observed at day 7 (MP1) and day 8 (MP2) is induced by phosphorus limitation, as modeled by Eq. (6.16). This simulation shows the model capability to perform a spatial analysis of biological processes and to assess their water depth dependence.

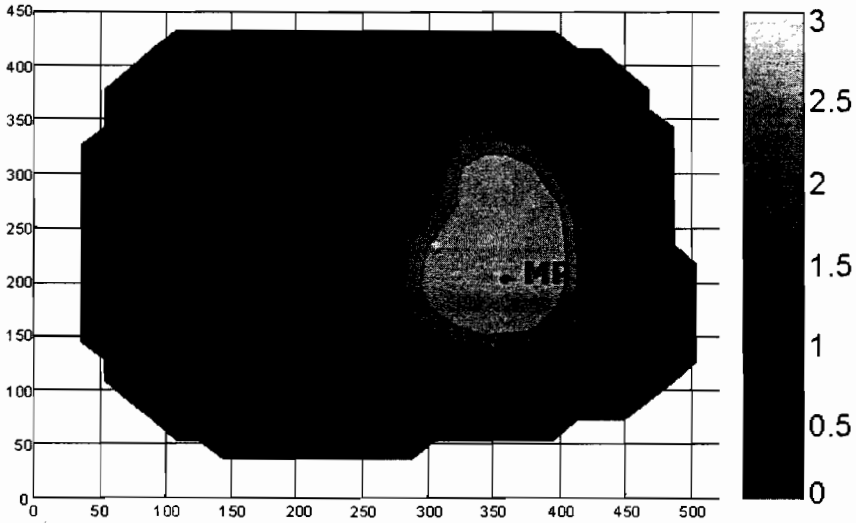


FIG. 8. Bathymetry of the shallow lake and monitoring points positioning used to demonstrate the SWAMP algae–nutrient dynamics.

VII. COUPLING THE WATER QUALITY MODULE WITH THE HYDRODYNAMIC MODEL

The previous example was concerned with the water quality model alone, though the hydrodynamic module was used to simulate diffusion. Now the computational linkage between the hydrodynamic and water quality parts is described in details. The relationship between the two modules is depicted in Fig. 11, showing that the combined computation of hydrodynamic and water quality variables is performed in a synchronous way. At each time step t , the concentration C is dynamically connected to the M_x , M_y , and h values. In fact, after the water depth $h(i, j)$ has been computed at nodes i and j using the continuity Eq. (3.1), the flow velocities u_x and u_y are obtained from flows M_x and M_y in the neighborhood of $h(i, j)$. In this way the water velocities in the two horizontal directions are spatially dependent on the same points of the h -grid. A mass

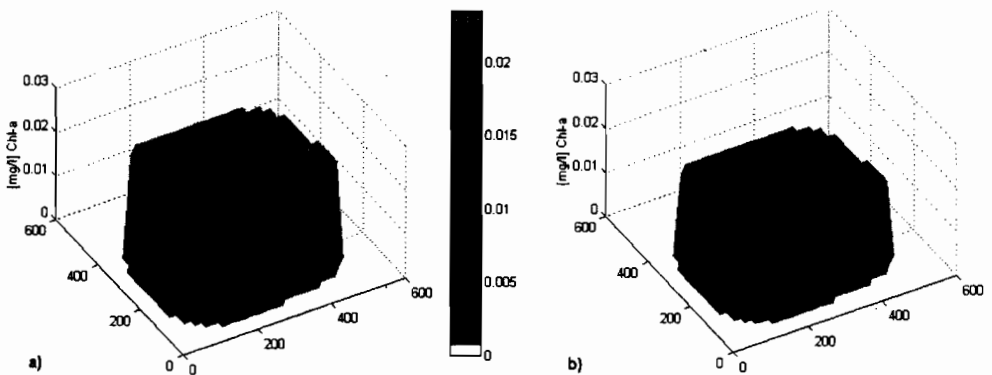


FIG. 9. Chlorophyll-*a* concentration after (a) $t = 6$ days and (b) $t = 10$ days.

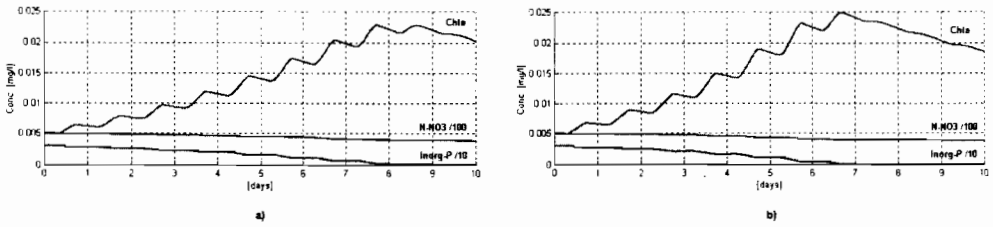


FIG. 10. Algae and nutrients evolution versus time for (a) monitoring point n.1 and (b) monitoring point n.2.

balance is then applied to these nodes and the concentration $C^i(i, j)$ is computed using the numerical algorithm already described. This concentration is representative not only of nodes i and j , but also of all points in the cell with sides D_x and D_y . Because the algorithm takes into account the four cells around the central element involved in the mass balance, the predictor-corrector method operates on a water quality grid consistent with the h -grid of the hydrodynamic module. To demonstrate the coupling between water quality and hydrodynamics, a simulation involving both aspects is presented. The same “U” shaped wetland of Sect. V.A. is considered, but this time a water quality module is linked to the basic hydrodynamic part. As in the previous algae-nutrients example of Sect. VI.E., literature values for the water quality parameters are used [9, 14]. Assuming the same hydraulic and diffusive conditions as in the tracer experiment of Section V.A, a constant dissolved BOD input of 30 mg/l is introduced at the inflow point. As initial conditions, zero dissolved BOD and a saturation DO value are assumed. The time evolution of these two variables are then shown in Fig. 12(a) at two monitoring points: MP1 (near the inlet) and MP2 (near the outlet). The simulation results are shown in Fig. 12(b) as a spatial plot of steady-state concentrations and in Fig. 12(c) as concentration vs. time at the monitoring points. Here, the time lag at MP2 introduced by the water flow is clearly discernible, until steady-state is eventually reached. Notice that in Fig. 12(c) the DO concentration at monitoring point MP2 shows a temporary oversaturation due to algae photosynthetic oxygen

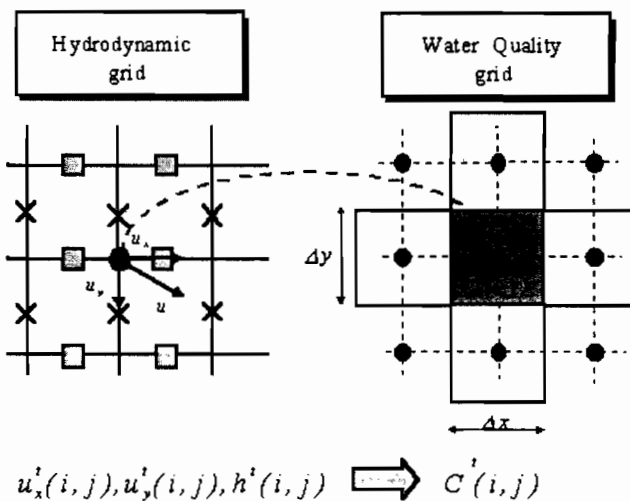
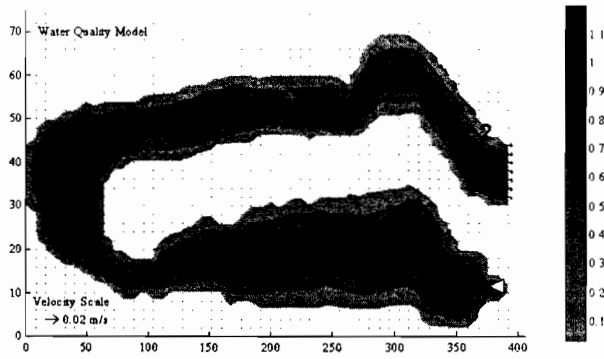
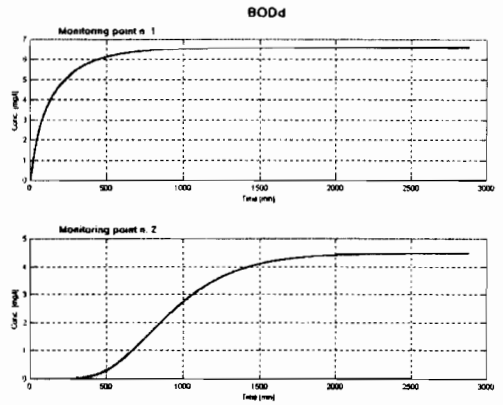


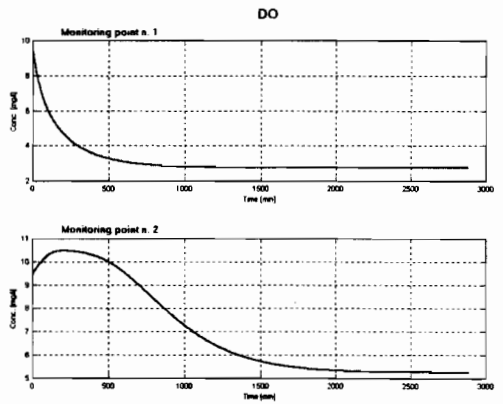
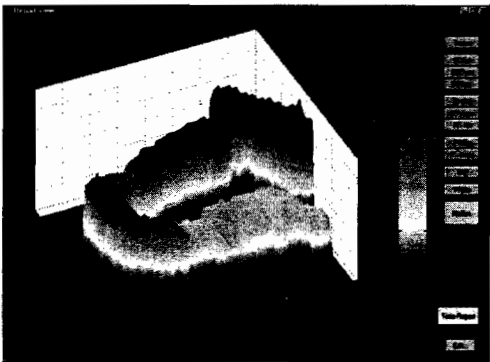
FIG. 11. Coupling the hydrodynamics and water quality computation.



a)



b)



c)

FIG. 12. (a) Location of monitoring points MP1 and MP2; (b) dissolved BOD plotted in space and time for the two monitoring points; (c) dissolved oxygen plotted in space and time for the two monitoring points.

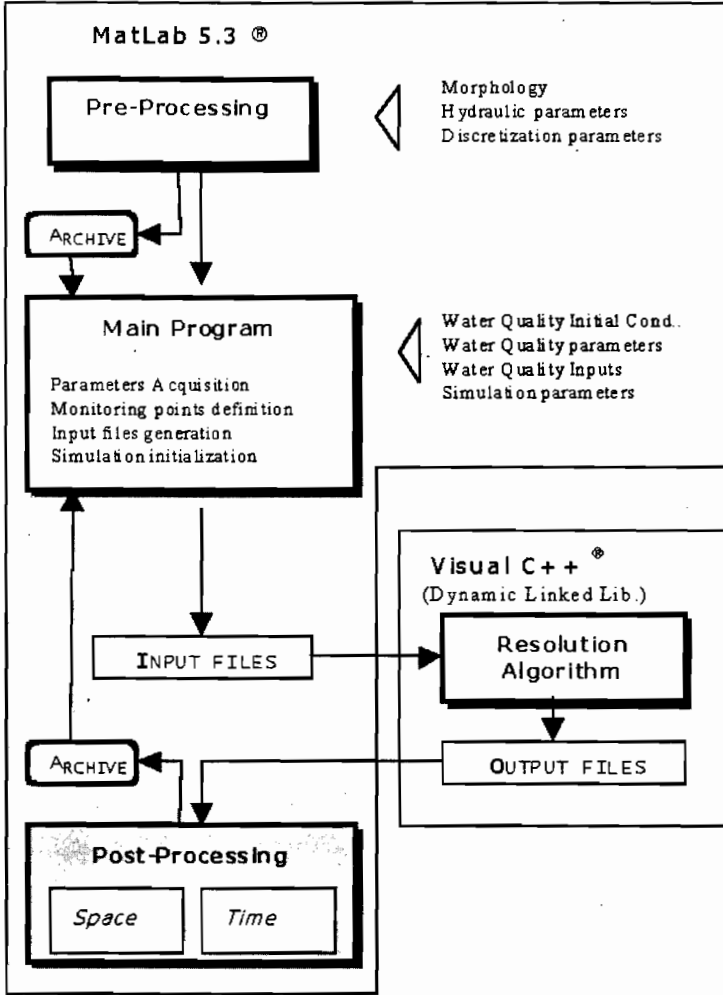
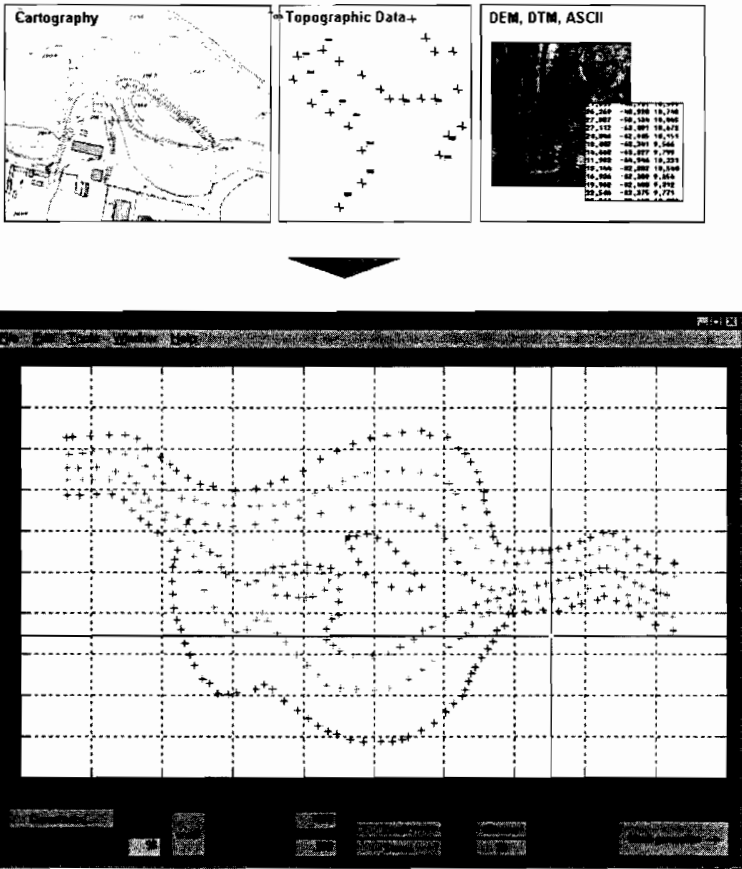


FIG. 13. Software engineering structure of SWAMP.

production in excess of uptake. It should be stressed that, as in the example of Section VI.E, the aim of the example was to demonstrate the feasibility of the combined model, and no attempt was made to simulate a real case-study, for which a specific calibration procedure would be required. The problem of adding a numerical calibration capability to SWAMP, readily available algorithms based on previous research [7] could be applied.

VIII. SOFTWARE ENGINEERING

Software engineering is one of the most relevant aspect of the bidimensional water quality model presented in this article. In two-dimensional analysis is often necessary to enhance the computational performance because of the large number of variables that need to be processed in comparison to the one-dimensional case. At the same time, an efficient user interface is



a)

FIG. 14. Preprocessing SWAMP sequence illustrating the steps through which the user is taken to enter data and define the problem set-up. [Figure is continued on next page.]

fundamental in handling multidimensional arrays such as morphological data, point-to-point basin, or water characteristics. In order to combine these aspects in an efficient and user-friendly way, the software environment must have both graphic capabilities and a powerful computational engine. SWAMP has been engineered using the MatLab 5.3 environment, where C++ subroutines can be compiled and linked as Dynamic Linked Library (DLL), whereas the graphical interface and input/output data handling is performed through standard MatLab functions. This architecture presents a simple front-end to the user, while maintaining its open framework features for the programmer, in terms of flexibility. The software engineering structure is shown in Fig. 13. The C++ subroutines implementing both the hydrodynamic and the quality modules are wholly transparent to the user. At the same time, the MatLab main program allows easy handling of the user interface and input-output data exchange. The most important tasks, apart from the computational engines described in the previous sections, are the pre- and postprocessing modules. The preprocessing module allows the reconstruction of the basin through a three-dimensional interpolation algorithm starting from morphological data. The digital terrain model is then transformed into a finite element grid and prepared for the

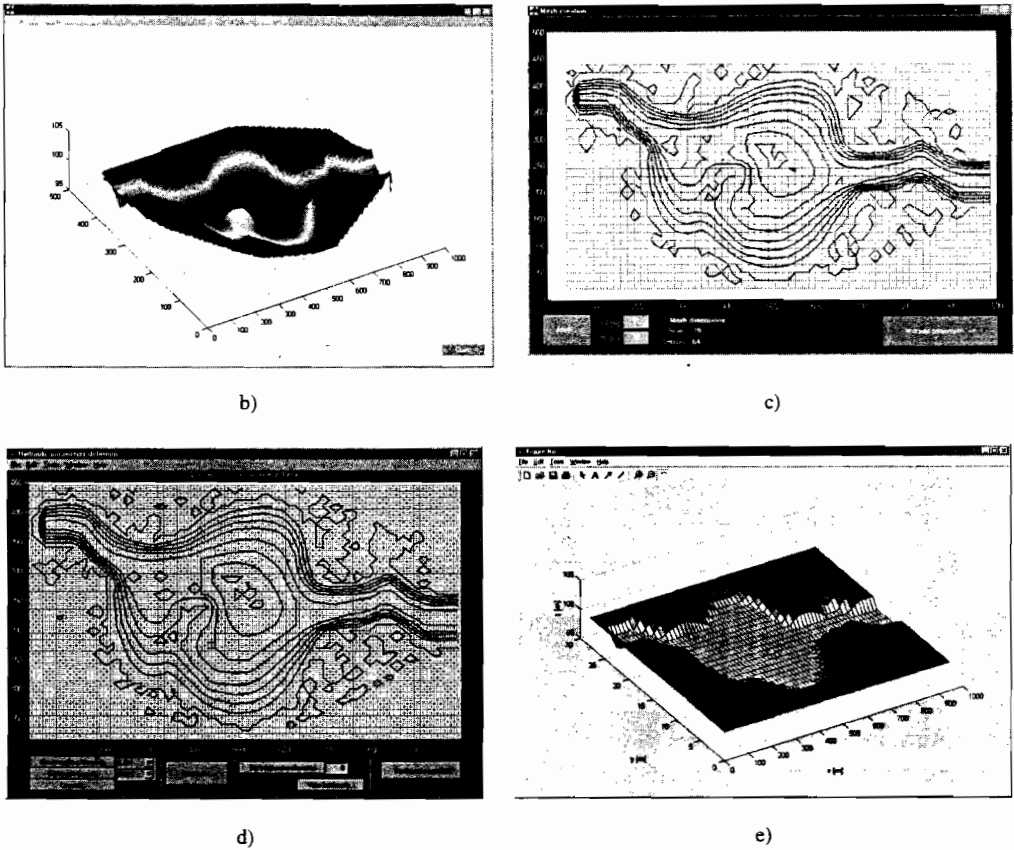


FIG. 14. (continued)

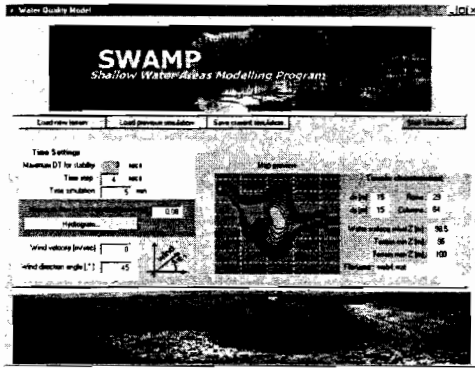
simulation by minimising the number of total mesh points. During this procedure all hydrodynamic parameters can be defined spatially to consider the effect of different bottom roughness for the hydraulic resolution. Figure 14 shows the typical preprocessing steps through which the user is guided by the graphical interface along the following steps.

Step 1 [Fig. 14(a)]. Topographic data can be acquired directly as numerical data (ASCII, DEM format) or digitized on-screen using a pointer device. The morphological data are stored as single points in three-dimensional space $P_n(x_n, y_n, z_n)$;

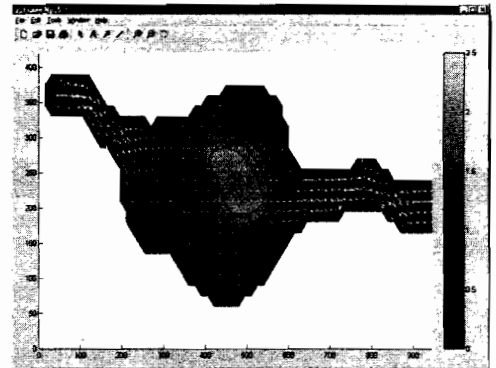
Step 2 [Fig. 14(b)]. Single spatial points are interpolated by the MatLab griddata procedure. The interpolation technique is based on Delaunay triangulation, which can be performed in a cubic, linear, or nearest mode;

Step 3 [Fig. 14(c)]. A rectangular finite elements mesh is generated dynamically by adjusting spatial discretization in the x and y directions. The user can view and interact with the finite element refinement so that computational effort and accuracy can be balanced. Mesh size is optimized to reduce total number of elements, ignoring areas with no morphological data;

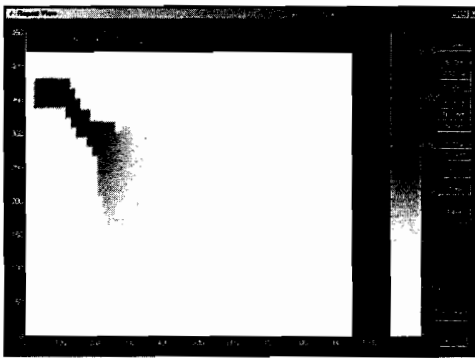
Step 4 [Fig. 14(d)]. Deals with the hydraulic characterization of the domain. A different Manning roughness coefficient can be assigned to each node so that local hydrodynamic friction



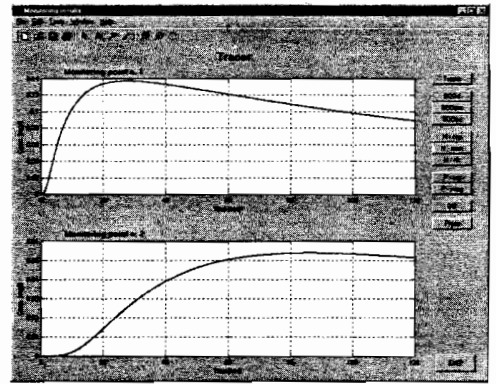
a)



b)



c)



d)

FIG. 15. Postprocessing SWAMP windows: (a) main program window; (b) hydrodynamic results; (c) spatial distribution of components; (d) concentration vs. time at monitoring points.

due to submerged macrophytes or bottom structures can be accounted for. Water sources and initial water surface elevation are also defined by the user in this step;

Step 5 [Fig. 14(e)]. The input file containing all the information required to perform a simulation is generated and saved. Now the problem is completely defined and hydrodynamic and water quality simulations can be performed.

All the information required for the simulation are controlled by the main SWAMP window in which forcing functions such as input mass and wind conditions can be defined together with the time-step size, compatible with the time-space step constraint of Eq. (3.12). Prior to a simulation, all the water quality specifications are directly entered or loaded from the archive of previous results, to be used as initial conditions. The simulation results are managed by the postprocessing module, which can display vector or three-dimensional representation of the hydrodynamic flux and component concentrations (Fig. 15). The dynamic evolution of state variables versus time can also be plotted at virtual monitoring points specified by the user. The graphical user interface is very useful in environmental analysis, where it is very important to perform a quick assessment of different possible scenarios on the same case study.

IX. CONCLUSIONS

In this article a two-dimensional water quality model named Shallow Water Analysis and Modelling Program (SWAMP) is presented. The major objective of the work is to create a comprehensive two-dimensional water quality model, based on an open modeling framework, combining easy programming of additional procedures with a simple user interface. The model was developed in the MatLab™ environment, using its Graphic User Interface, whereas proprietary DLL obtained from C++™ subroutines were used for the main resolution algorithms. This implementation enhanced the computational performance of the model by reducing the run-time by two orders of magnitude compared to plain MatLab implementation. A tracer study based on experimental data and a comparison with MIKE21 model were used to assess the hydraulic and advection-diffusion modules. Both tests show that SWAMP can reliably fit the tracer response, in terms of pulse shape and mass conservation with minimum calibration effort, although the morphology of the case study at hand is not particularly suited for a two-dimensional computational scheme, given its elongated form. More simulations are presented to test the water quality module. They are produced using literature parameter values of sufficient generality [9, 11, 14]. In this regard it should be noted that the aim of the work is to build an efficient user interface around a known set of environmental kinetics to produce a self-contained water quality analysis package. Therefore, the scope of these examples is to demonstrate the feasibility of the combined model, and no attempt is made here to any real case-study, for which a specific calibration procedure would be required. Therefore the assessment should be made in terms of computational accuracy, interface efficiency, and easiness of use rather than a particular system response. In this sense, it can be concluded that a robust, simple, and unified user interface has been achieved, leading even the nonexpert user through all the steps needed to define and simulate a shallow water quality problem and to present the results in a clear and intelligible way.

APPENDIX

Nomenclature

α	angle between the x axis and wind direction (deg)
a_{na}	nitrogen to chlorophyll- a ratio
a_{pa}	phosphorus to chlorophyll- a ratio
$a_{w,x}$	wind-induced acceleration term in the x direction (m/s^2)
$a_{w,y}$	wind-induced acceleration terms in the y direction (m/s^2)
BOD_d	dissolved biochemical oxygen demand ($mg\ O_2/l$)
BOD_p	particulate biochemical oxygen demand ($mg\ O_2/l$)
BOD_s	settled biochemical oxygen demand ($mg\ O_2/l$)
C	generic pollutant concentration (mg/l)
C_i	exogenous loading rate for the generic pollutant ($mg\ l^{-1}\ day^{-1}$)
c_d	dimensionless drag coefficient
δ	algal preference for nitrate-N over ammonium-N
D_x	diffusion coefficient in the x direction (m^2/s)
D_y	diffusion coefficient in the y direction (m^2/s)

f	photoperiod
φ_l	attenuation of growth due to light (-)
G_{max}	maximum plant growth rate (day^{-1})
I_a	instantaneous light intensity ($\text{cal cm}^{-2} \text{day}^{-1}$)
I_s	optimal light intensity for plant growth ($\text{cal cm}^{-2} \text{day}^{-1}$)
K_e	light extinction coefficient (m^{-1})
K_b	dissolved BOD decay rate (day^{-1})
K_d	algae decay rate (day^{-1})
$K_{deg\text{sed}}$	settled BOD decay rate (day^{-1})
K_{denit}	denitrification maximum reaction rate (day^{-1})
K_g	algae growth rate (day^{-1})
$K_{g,20}$	algae growth rate at 20°C (day^{-1})
K_{hydr}	particulate BOD hydrolysis rate (day^{-1})
K_N	N-half saturation constant for algae growth (mg/l)
K_{nit}	maximum reaction rate for nitrification (day^{-1})
K_{min}	mineralization rate of organic nitrogen (day^{-1})
K_{NO_3}	DO-inhibition constant for denitrification (mg/l)
K_P	Phosphorus half saturation constant for algae growth (mg/l)
K_O	DO-half saturation constant for nitrification (mg/l)
K_{ra}	algae respiration rate (day^{-1})
K_{rear}	recreation rate (day^{-1})
K_{sed}	phosphorus settling rate (day^{-1})
$K_{sed\text{phyt}}$	algae sedimentation rate (day^{-1})
h	water depth (m)
H	total surface elevation above a reference height (m)
θ_b	temperature correction coefficient
M_x	mass flow in the x direction (m^3/s)
M_y	mass flow in the y direction (m^3/s)
n	Manning roughness coefficient
ρ_a	air density (kg/m^3)
P_{phyt}	photosynthetic oxygen production rate (day^{-1})
r_{oa}	photosynthetic oxygen production ratio
R_{phyt}	algae oxygen consumption rate for respiration (day^{-1})
$R_{c\text{phyt}}$	algae growth rate for combined N-P availability (day^{-1})
R_{sed}	sediment oxygen demand ($\text{mg l}^{-1} \text{day}^{-1}$)
u_{crit}	critical velocity for resuspension (m day^{-1})
u_x	flow velocity in the x direction (m/s)
u_y	flow velocity in the y direction (m/s)
v_{sed}	particulate BOD settling velocity (m day^{-1})
v_{ris}	settled BOD resuspension velocity (m day^{-1})
$v_{ris\text{max}}$	maximum settled BOD resuspension velocity (m day^{-1})

The authors acknowledge the cooperation of Prof. G. Bendoricchio, Department of Industrial Chemistry, University of Padua, Italy, and his work-group in supplying the data for the experimental tracer study and of Dr. L. Cappiotti, Department of Civil Engineering, University of Florence, for setting up the MIKE21 simulations.

References

1. H. Wang and R. A. Falconer, Simulating disinfection processes in chlorine contact tanks using various turbulence models and high-order accurate differences schemes, *Water Res* 32 (1998), 1529–1543.
2. J. Wu, Wind stress and surface roughness at air-sea interface, *J Geophys Res* 74 (1969), 444–445.
3. Y. Wu and R. A. Falconer, A mass conservative 3-D numerical model for predicting solute fluxes in estuarine waters, *Adv Water Res* 23 (2000), 531–543.
4. R. W. Mac Cormack, The effect of viscosity in hypervelocity impact cratering, *Am Inst Aeronaut Astronaut*, New York, 1969, Paper 69–354.
5. Y. Iwasa and K. Inoue, Mathematical simulations of channel and overland flood flows in view of flood disaster engineering, *J Nat Disaster Sci* 4 (1982), 1–30.
6. M. Yan and R. Kahawita, Modelling the fate of pollutant in overland flow, *Water Res* 34 (2000), 3335–3344.
7. S. Marsili-Libelli, Parameter Estimation of Ecological Systems, *Ecol Modelling* 62 (1992), 233–258.
8. A. Okubo, Oceanic diffusion diagrams, *Deep-sea Res* 18 (1971), 789–802.
9. S. C. Chapra, *Surface Water-Quality Modeling*, McGraw Hill, New York, 1997.
10. M. J. Gromiec, D. P. Loucks, and G. T. Orlob, Stream quality modeling, G. T. Orlob, editor, *Mathematical Modelling of Water Quality*, Wiley, IIASA n. 12, 1983, Cap. 6.
11. G. L. Bowie, W. B. Mills, D. B. Porcella, C. L. Campbell, J. R. Pagenkopf, G. L. Rupp, K. M. Johnson, P. W. H. Chan, S. A. Gherin, Rates, constants, and kinetics formulations, *Surface Water Quality Modeling* (2nd ed.), EPA/600/3-85/040, EPA Environmental Research Laboratory, Athens, GA, 1985.
12. R. V. Thomann and J. A. Mueller, *Principles of Surface Water Quality Modeling and Control*, Harper Int., 1987.
13. R. B. Ambrose, T. A. Wool, J. L. Martin, WASP5, A Hydrodynamic and Water Quality Model, Model Theory, User's Manual, U. S. Environmental Protection Agency, Athens, GA, 1993.
14. L. Brown and T. O. Barnwell, The enhanced stream water quality models QUAL2E and QUAL2E-UNCAS: documentation and user manual, Environmental research laboratory U.S. E.P.A, report EPA/600/3-87/007, Athens, Georgia, 1987.